Dear author,

Please note that changes made in the online proofing system will be added to the article before publication but are not reflected in this PDF.

We also ask that this file not be used for submitting corrections.

Lithos xxx (xxxx) xxx

Contents lists available at ScienceDirect

Lithos

journal homepage: www.elsevier.com/locate/lithos

Anticlockwise P-T evolution of amphibolites from NE Sardinia, Italy: Geodynamic implications for the tectonic evolution of the Variscan Corsica-Sardinia block

Scodina M. [a], Cruciani G. [a], Franceschelli M. [a,*], Massonne H.-J. [b]

[a] Dipartimento di Scienze Chimiche e Geologiche, Università degli Studi di Cagliari, Cagliari, Italy
[b] Institut für Mineralogie und Kristallchemie, Universität Stuttgart, Stuttgart, Germany

ARTICLE INFO

Article history:
Received 3 September 2018
Accepted 6 December 2018
Available online xxxx

Keywords:
Amphibolite
Garnet zoning
Metamorphic evolution
P-T pseudosection
Counterclockwise P-T path
Variscan Sardinia

ABSTRACT

In the Migmatite Complex from NE Sardinia, a large lensoid body of coarse-grained, dark-green amphibolite with a schistose to weakly massive aspect crops out. Within this amphibolite centimetre-sized layers locally occur which contain millimetric porphyroblastic garnet. We investigated the amphibolite and the layers applying microstructural analyses and thermodynamic modelling in the NCKFMASH+Ti + Mn system in order to reconstruct the pressure-temperature (P-T) metamorphic evolution. The amphibolite underwent a burial path, recorded by the compositional zoning of garnet, that started at pressures of 0.8 GPa and showed only a slight increase in temperature leading to peak P-T conditions. The garnet rim records peak P-T conditions of 1.3–1.4 GPa at 690–740 °C. As the early exhumation of the amphibolites occurred already at lower temperatures than the burial, an anticlockwise P-T path results which is in contrast to the typical clockwise P-T paths reported for several high-pressure metamorphic rocks from NE Sardinia. We interpret the anti-clockwise path by the location of the studied rocks in the lowermost part of the upper plate and their burial to depths of around 45 km during the Variscan continental collision between Laurussia and Gondwana. This process could have affected some rock slices of the upper plate only owing to tectonic erosion by the downgoing plate. The subsequent uplift occurred in an exhumation channel where these slices were continuously cooled by the upper portion of the lower continental plate.

1. Introduction

The knowledge and comprehension of metamorphic processes, especially the contrasting evolution of low- and high-pressure (HP: > 1.0 GPa) rocks of the Sardinian-Corsican basement (e.g. Cruciani et al., 2013; Giacomini et al., 2008; Massonne et al., 2018), is considered to be of high relevance for a better understanding of the dynamics of the Variscan continent-continent collision. The corresponding information can be gathered from studies related to the reconstruction of pressure (P)-temperature(T)-time(t)-deformation(d) paths using modern geochemical and petrological methods (e.g. Cruciani et al., 2013, 2014a, 2018; Massonne, 2016a; Massonne et al., 2018). A major issue of the Sardinian-Corsican basement rocks is the relationship between metabasic bodies and the enclosing metasedimentary and meta-igneous host rocks. Understanding this relationship is very important because different interpretations have different implications on the tectonic evolution of the Variscan belt (Cruciani et al., 2013, 2015a).

Within the migmatites and orthogneisses of the Migmatite Complex of the Inner Zone of the Variscan Sardinian belt (Fig. 1), several decametric to hectometric basic and ultrabasic lenticular bodies occur. These bodies are characterized by a multi-facies evolution, with evidence of an early stage at high temperature (granulitic) or high pressure (eclogitic). Basic bodies with granulite-facies relics are those of Mt. Nieddu north of the town of Olbia (Cruciani et al., 2002; Ghezzo et al., 1979) and Punta Scorno in the Asinara island (Carosi et al., 2004; Castorina et al., 1996). These bodies were interpreted by the cited authors as layered basic igneous rocks (with chemical features similar to tholeiites) which intruded the lower crust and experienced a retrograde metamorphic evolution. In this paper, we present results of the investigation of amphibolites from Mt. Nieddu in order to reconstruct their early metamorphic evolution and the subsequent pressure-temperature (P-T) path mainly through garnet compositional zoning. In fact, these rocks, due to a massive amphibolite-facies overprint which locally transformed the original rock into an aggregate of amphibole, plagioclase and quartz ± ilmenite, broadly lack relics of early stages of the metamorphic history, but the integration of geological, petrographic and thermodynamic data allowed us to reconstruct the early stages of the P-T metamorphic evolution and to include these

* Corresponding author.
E-mail address: francmar@unica.it (M. Franceschelli).

https://doi.org/10.1016/j.lithos.2018.12.003
0024-4937/© 2018 Elsevier B.V. All rights reserved.

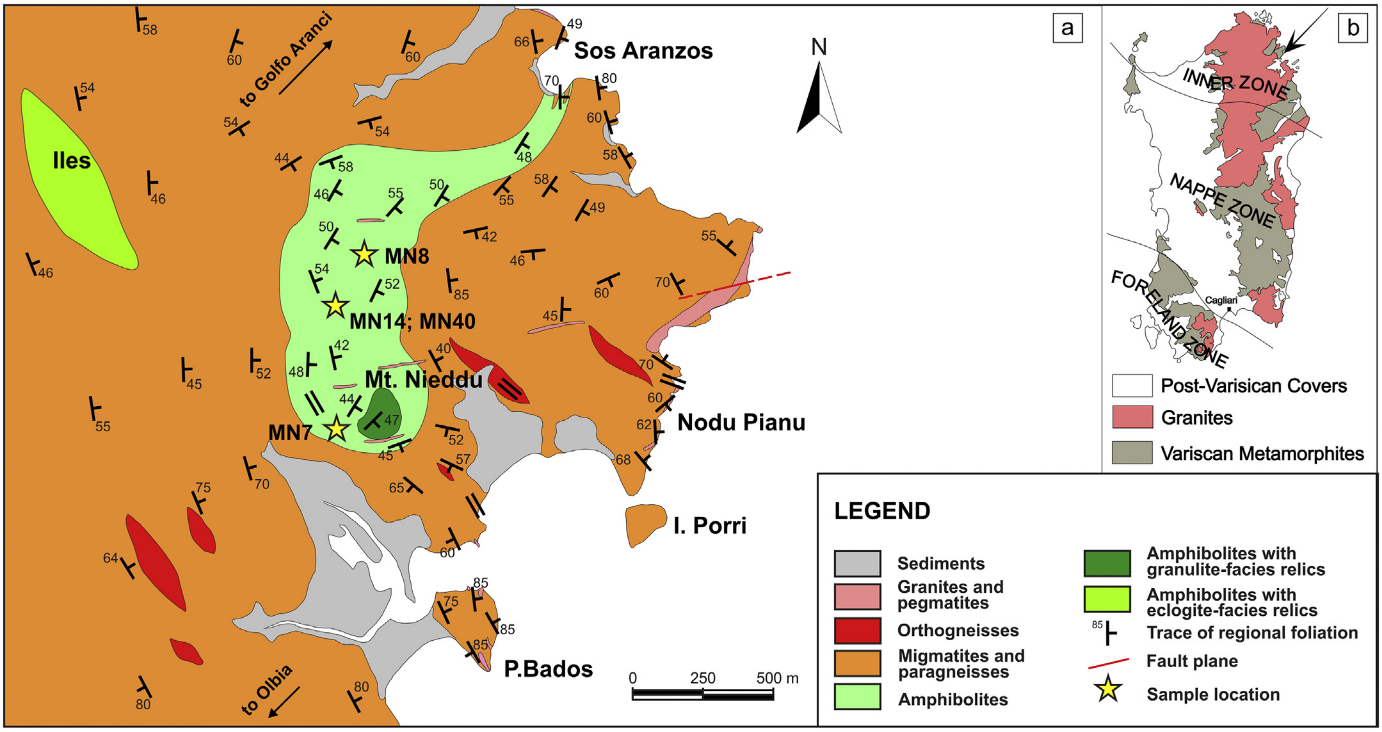

Fig. 1. (a) geological sketch map of the Golfo Aranci area. The inset (b) shows a simplified tectonic sketch map of the Sardinian Variscan chain. Arrow in (b) shows the study area.

rocks in the continent-continent collisional context of the Variscan orogeny. The studied rocks are characterized by an anticlockwise P-T path, which might be typical for rocks that belong to the lowest portion of the upper plate and are involved in an exhumation channel (Massonne et al., 2018). On the contrary, typical clockwise P-T paths, documented for several HP metamorphic rocks from NE Sardinia (Cruciani et al., 2012, 2013; Franceschelli et al., 2007; Giacomini et al., 2005a), refer to the upper portion of the downgoing plate. Both rock types with different character of the P-T path are now exposed in tectonic contact in the Inner Zone of the Sardinian metamorphic basement probably as a result of the exhumation process in Carboniferous times.

2. Geological setting and field occurrence

The Golfo Aranci area, located north of Olbia, belongs to the Migmatite Complex (also known as High Grade Metamorphic Complex = HGMC), which is part of the Inner Zone of the Variscan Sardinian belt that also extends to southern Corsica. The corresponding metamorphic basement, which resulted from the Variscan orogeny during late Palaeozoic times, has experienced several deformation phases (see Franceschelli et al., 2005a, Helbing et al., 2006 for in-depth analyses) and has been divided by several authors into three main tectono-metamorphic zones, with an increasing metamorphic grade from the southern External Zone (foreland zone in Fig. 1 inset) throughout the Nappe Zone to the Inner Zone in the northernmost part of Sardinia (Carmignani et al., 1994, 2001).

According to Carmignani et al. (1994, 2001) the Inner Zone consists of two different metamorphic complexes: (i) the High-Grade Metamorphic Complex (HGMC, or Migmatite Complex) below described in detail; (ii) the Medium-Grade Metamorphic Complex (MGMC) consisting of micaschist and paragneiss, with a Barrovian sequence towards the north (Franceschelli et al., 1982), including boudins of quartzite and metabasalt with N-MORB signature (Cappelli et al., 1992).

The contact between the two complexes, well exposed in the Posada valley, southern Gallura and Asinara island (Carosi et al., 2005, 2009; Oggiano and Di Pisa, 1992), runs along a transpressional shear zone that was active between 320 and 310 Ma (Di Vincenzo et al., 2004; Carosi and Palmeri, 2002; Iacopini et al., 2008; Carosi et al., 2012). An extended and detailed review of the Variscan orogeny in Sardinia can be found in Carmignani et al. (2001 and references therein), Rossi et al. (2009), Franceschelli et al. (2005a), and Cruciani et al. (2015b). Variscan tectono-metamorphic events accompanied by the emplacement of intrusive rocks in the time span between 320 and 280 Ma (Casini et al., 2012). The metamorphic basement is unconformably covered by Late Carboniferous–Early Permian sedimentary rocks filling extensional basins (Barca et al., 1995; Carmignani et al., 1994).

The HGMC consists mainly of polydeformed sedimentary-derived gneisses and migmatites (Cruciani et al., 2014a, 2014b; Massonne et al., 2013), which reached a high metamorphic grade (sillimanite + K-feldspar zone, Franceschelli et al., 2005a). According to Giacomini et al. (2006) the high-grade complex principally consists of metamorphosed middle Ordovician granitoids associated with a thick sedimentary sequence characterized by a maximum age of deposition between 480 and 450 Ma. A middle Ordovician age for the migmatitic igneous protolith was also obtained by Cruciani et al. (2008). Subordinate rocks of the HGMC are orthogneisses, calc-silicate nodules and metabasite lenses (basic and ultrabasic rocks with eclogite and granulite facies relics, Franceschelli et al., 1998, 2002, 2005b, 2007; Cruciani et al., 2010, 2011, 2015b). These lenses are elongated parallel to the regional schistosity (Franceschelli et al., 2005a).

In north Sardinia, a polyphase deformation was characterized by Franceschelli et al. (1982), Connolly et al. (1994), and Carosi et al. (2005) as follows. The D_1 collision-related deformation is well-recorded in the L-MGMC, where it is associated with a penetrative S_1 axial plane foliation of SW-facing folds (Carosi et al., 2004; Carosi and Oggiano, 2002; Montomoli, 2003). Late D_1 ductile/brittle shear zones, with top to the SW sense of movement, overprint F_1 folds. Towards north the S_1 foliation is progressively transposed by the D_2 phase, which is associated with upright up to NE verging folds and dextral shear zones. The large NW-SE trending shear belt (former Posada-Asinara Line) that separates the HGMC from the L-MGMC is characterized by dextral shearing, which is in turn anticipated by D_2 sinistral shear movements. The D_2 transpressional deformation is related to the NNE-SSW compression and the NW-SE shear displacement (Carosi

Please cite this article as: M. Scodina, G. Cruciani, M. Franceschelli, et al., Anticlockwise P-T evolution of amphibolites from NE Sardinia, Italy: Geodynamic implications for the..., Lithos, https://doi.org/10.1016/j.lithos.2018.12.003

et al., 2004, 2005, 2009; Carosi and Oggiano, 2002; Carosi and Palmeri, 2002; Iacopini et al., 2008). A D_3 deformation phase forming upright metric to decametric open folds developed subsequently. F_3 folds are associated with an S_3 axial plane crenulation cleavage. The D_4 tectonic phase is revealed by metric to decametric folds with sub-horizontal axial planes (Cruciani et al., 2015b and references therein).

The studied rocks are located a few kilometres NE of Olbia (Mt. Nieddu locality; Fig. 1) where a large lensoid amphibolite body, 2 km long in NE-SW direction and 100–150 m wide, crops out. Within this body a smaller body of dark green to black ultrabasic amphibolites occurs, in which granulite facies relics have been recorded (Cruciani et al., 2002; Franceschelli et al., 2002). The most foliated rocks of the amphibolite body are located at the edge of this body near the contact to the migmatite and show a typical banded (flaky) structure with an alternation of centimetric to decimetric white, plagioclase-rich and dark green, amphibole-rich bands (Fig. 2a). The plagioclase-rich bands are frequently folded and boudinaged. In the amphibolite body several white to greenish millimetric to centimetric epidote-rich veins and, locally, centimetre-thick layers containing up to 1 cm large garnet porphyroblasts surrounded by a matrix of amphibole and a fine-grained symplectite-type microstructure (Fig. 2b,c) occur. These garnet-bearing layers are oriented parallel to the main S_2 regional schistosity (Fig. 2a, b). The contact with the surrounding migmatites is tectonic and slightly discordant from the main regional foliation.

The hosting migmatites are coarse-grained rocks with stromatic fabric and a well-developed foliation derived from an original psammitic to pelitic sequence. All metamorphic rock types in the study area are crosscut by discordant metre-sized dykes of leucogranitic composition.

3. Analytical methods

Mineral assemblages and microstructures of selected samples of the amphibolites from Mt. Nieddu were investigated by optical and scanning electron microscopes at the Dipartimento di Scienze Chimiche e Geologiche, Università di Cagliari. For this purpose, carbon-coated polished thin-sections were used.

The chemical composition of the main rock-forming minerals was determined with a CAMECA SX100 electron microprobe (EMP) equipped with five wave-length dispersive (WD) spectrometers at the Institut für Mineralogie und Kristallchemie, Universität Stuttgart. The operative conditions included 15 kV acceleration voltage, 15 (garnet) or 10 nA (other silicates, ilmenite) beam current, and a 5 μm spot size. For the description of the used standards, counting times and analytical errors see Massonne (2012). Structural formulae were calculated on the basis of 12, 6, and 8 oxygen anions for garnet, pyroxene, and plagioclase, respectively. The amphibole structural formula was calculated for 23 oxygen anions using the CalcMin program (Brandelik, 2009).

Major elements of some selected whole-rock samples were determined with the WD system of a PHILIPS PW2400 X-ray spectrometer (XRF) at the Institut für Mineralogie und Kristallchemie, Universität Stuttgart. For this purpose, a glass disc was previously prepared by fusing rock powder with Spectromelt® (ratio 1:6).

4. Petrological investigation

4.1. Petrography

On the basis of microstructural relationships and textural features we recognized that the garnet-bearing layers records the early metamorphic history of the amphibolites (stage 1 and respective substages a-f, Fig. 3) whereas the mineral assemblage of the hosting rock (stage 2) represents the subsequent retrograde re-equilibration. The local growth of late phases in both garnet-bearing layers and host amphibolites testifies a later re-equilibration stage (stage 3). Stage 1 has been in turn subdivided into the following substages: a, b, c) garnet core (e.g. = Grt_{1a}), mantle and rim, respectively, with their inclusions; d) minerals in symplectite-like texture; e) minerals in the corona around garnet; f) minerals in the matrix of the garnet-bearing layer. A scheme of the metamorphic evolution history is represented in Fig. 3.

The garnet-bearing layers inside the amphibolites (samples MN14A, MN40) are characterized by the presence of several mm-sized garnet porphyroblasts (Grt, Figs. 2 and 4) in a matrix made up of amphibole (Amp_{1f}) and plagioclase (Pl_{1f}), quartz and flakes of a fine-grained symplectite of clinopyroxene (Cpx_{1d}) + plagioclase (Pl_{1d}) (Fig. 4e). These flakes are generally slightly curvilinear and elongated parallel to the regional S_2 schistosity (Fig. 4a). Garnet can reach a maximum of

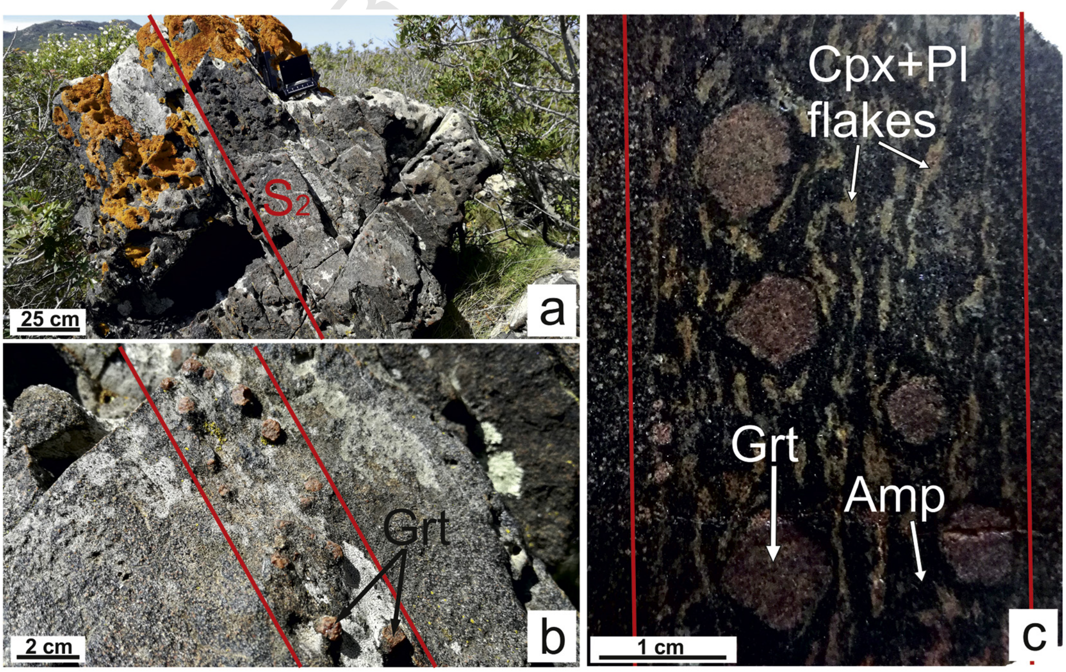

Fig. 2. (a) Field photograph of the Mt. Nieddu amphibolites (Golfo Aranci area); the red line indicates the direction of the regional foliation (S_2). (b) Photograph of a garnet-bearing layer in the amphibolites; (c) Cut and polished hand-sample of a garnet-bearing layer in the amphibolites of Mt. Nieddu. Grt = garnet; Cpx = clinopyroxene; Pl = plagioclase; Amp = amphibole. (For interpretation of the references to colour in this figure legend, the reader is referred to the web version of this article.)

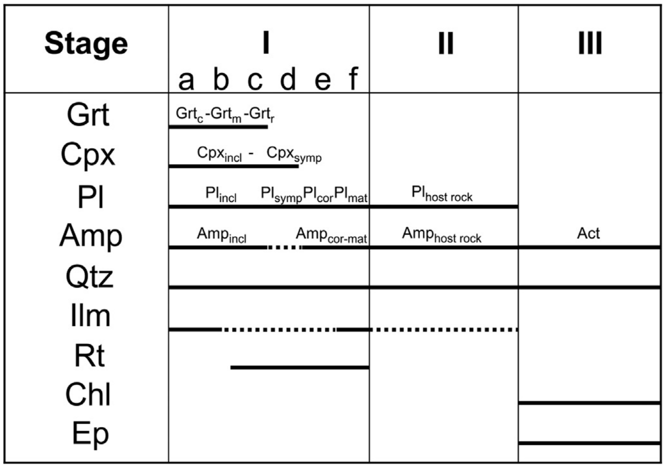

Fig. 3. Metamorphic evolution scheme deduced from microstructures in garnet-bearing layers of amphibolites from the Golfo Aranci. Grt = garnet; Cpx = clinopyroxene; Pl = plagioclase; Amp = amphibole; Act = actinolite; Qtz = quartz; Ilm = ilmenite, Rt = rutile; Chl = chlorite; Ep = epidote. Stage I: mineral paragenesis in garnet-bearing layer; Stage II: mineral assemblage in the hosting rock; Stage III: later re-equilibration stage. Substages a, b, c: garnet core, mantle and rim, respectively, and their inclusions; d) minerals assemblage in symplectite-like texture; e) mineral assemblage in corona around garnet; f) mineral assemblage in the garnet-bearing layer matrix.

30 vol% in the garnet-rich layers and contains inclusions of amphibole ($Amp_{1a\text{-}b\text{-}c}$), plagioclase ($Pl_{1a\text{-}b\text{-}c}$), quartz, minor clinopyroxene ($Cpx_{1a\text{-}b\text{-}c}$), and ilmenite ($Ilm_{1a\text{-}b\text{-}f}$) (Fig. 4d). The interface between garnet and the surrounding layer matrix is marked by a thin sub-millimetric coronitic rim made up of plagioclase (Pl_{1e}) and amphibole (Amp_{1e}) (Fig. 4b, c). Pl_{1e} rimming garnet is locally sericitized. Amp_{1e} and Amp_{1f} can be zoned with a retrograde phase (actinolite, Amp_3) growing at its margin. The matrix contains also relevant modal amounts of plagioclase (Pl_{1f}), quartz, ilmenite (Ilm_{1f}), and rare clinopyroxene (Cpx_{1f}) (Fig. 4f). In the proximity of garnet the elongation of Amp_{1f} follows the direction of the euhedral faces of garnet. Accessory minerals in the garnet-bearing layers are zircon, rutile, titanite, apatite, K-feldspar, chlorite, Fe-oxides, monazite, and biotite. Rutile grains occur in both garnet ($Rt_{1b\text{-}c}$) and matrix (Rt_{1f}). $Rt_{1b\text{-}c}$ with sizes between 10 and 30 μm is smaller than Rt_{1f} which is usually larger than 70–80 μm. Rt_{1f} can show a rim of titanite or a partial replacement by ilmenite.

The amphibolites of Mt. Nieddu (hosting rock, stage 2) are characterized by a coarse-grained granoblastic texture with a slight crystal anisotropy (samples MN7, MN8). The most abundant phase (≥50 vol %) is green amphibole (Amp_2) due to the strong metamorphic re-equilibration in the amphibolite facies partially erasing igneous phases and previous metamorphic mineral parageneses. Its size ranges from sub-millimetric to millimetric. Plagioclase of stage 2 (Pl_2) is generally idioblastic and can reach modal amounts of 50–70 vol% in white bands and 20–30 vol% in dark-green bands. Quartz, epidote (Ep_3) and chlorite (Chl_3) occur in variable modal amounts (from 1 to 15 vol%). Ep_3 appears as millimetric to sub-millimetric veins or small patches. Accessory minerals are clinopyroxene, apatite, ilmenite, zircon, monazite and minor calcite.

4.2. Mineral chemistry

Selected microprobe analyses of garnet, pyroxene, plagioclase, amphibole, ilmenite, epidote and chlorite from samples MN14A and MN40 of the garnet-bearing layers and from samples MN7 and MN8 of the host amphibolites are reported in Tables 1 to 5. The location of these samples is illustrated in Fig. 1.

Garnet is almandine rich (56–59 mol%) and spessartine poor with intermediate pyrope and constant grossular (27 mol%) contents. From core to rim almandine contents slightly increase, pyrope contents increase from 10 to 16 mol%, and spessartine contents decrease from 7 to 1 mol%. Due to the absence of definite compositional layers we decided to arbitrarily define the core, the mantle and the rim of selected garnets by using the molar content of Mn and Mg (garnet core = $X_{Mn} > 0.04$, $X_{Mg} < 0.11$; garnet mantle = $0.02 > X_{Mn} > 0.04$; $0.11 > X_{Mg} > 0.13$; garnet rim = $X_{Mn} = 0.01$; $X_{Mg} > 0.13$). Compositional X-ray maps (Ca, Mg, Fe, Mn) of selected garnets from MN14A and MN40 samples are shown in Fig. 5.

Cpx_{1a} is diopside with X_{Na} [= Na/(Na + Ca)] values of 0.06–0.07 and X_{Mg} [= Mg/(Mg + Fe)] between 0.62 and 0.66. Cpx_{1c} differs from Cpx_{1a} by a slightly lower X_{Na} value of 0.05–0.06. Cpx_{1d} is also diopside with a very narrow range of X_{Na} and X_{Mg} values (0.04–0.05 and 0.71–0.72, respectively). Cpx_{1f} is characterized by $X_{Na} = 0.05$ and $X_{Mg} = 0.70$.

$Pl_{1a\text{-}c}$ is andesine with X_{Na} values between 0.65 and 0.69. Pl_{1d} and Pl_{1e} show slightly higher X_{Na} values of 0.68–0.69 and 0.70–0.73, respectively. Pl_{1f} is oligoclase with X_{Na} between 0.80 and 0.84. Pl_2 is bytownite with X_{Na} between 0.14 and 0.16.

Amphibole is only calcic according to Leake et al. (1997). $Amp_{1a\text{-}c}$ is tschermakite to tschermakite-hornblende with Si = 6.1 to 6.3 atoms per formula unit (apfu) and X_{Mg} = 0.77 to 0.83. Amp_{1e} is tschermakite-hornblende with Si = 6.3 apfu and X_{Mg} = 0.74–0.75. Amp_{1f} is tschermakite and tschermakite-hornblende with Si = 6.2–6.3 apfu and X_{Mg} = 0.80–0.84. Amp_2 is Mg-hornblende with Si = 6.9–7.0 apfu and X_{Mg} = 0.79–0.81. Amp_3 is actinolite with Si contents ranging from 7.7 to 7.9 apfu and X_{Mg} between 0.5 and 0.7 and actinolite-hornblende with Si = 7.4 apfu and X_{Mg} = 0.64.

Ilm_{1ab} differs from Ilm_{1f} by a larger content in MnO (1.0 wt% for Ilm_{1ab} vs. 0.33 for Ilm_{1f}) and a slightly higher content in MgO (0.05 wt % for Ilm_{1ab} vs. 0.04 for Ilm_{1f}). Ep_3 is characterized by variable trivalent iron contents ranging from 0.25 to 0.50 apfu. Chl_3 is clinochlore with Si = 5.7 apfu and a Fe content of 1.7 apfu. Rutile grains (Rt_{1c}) included in the garnet rim are characterized by ZrO_2 contents ranging from 0.02 to 0.06 wt% and rutile grains from layer matrix (Rt_{1f}) from 0.05 to 0.09 wt%.

5. Pressure-temperature evolution

5.1. P-T pseudosection modelling

We calculated P-T pseudosections for samples MN14A, MN40, MN7 and MN8 (Fig. 6 and Supplementary Fig. S1) in order to reconstruct the evolution of the metamorphic history based on, for instance, the garnet compositional zoning. The P-T pseudosections were calculated in the NCKFMASH+Ti + Mn system using the software PERPLE_X (Connolly, 1990, 2009) and the thermodynamic data set of Holland and Powell (1998, updated 2002 and 2004) for H_2O and minerals. The used solid-solution models are those of Holland and Powell (1998: garnet, white mica, epidote), Holland and Powell (1996: orthopyroxene), Green et al. (2007: clinopyroxene), Holland et al. (1998: chlorite), Powell and Holland (1999: biotite, potassic white mica), Dale et al. (2005: amphibole), and Newton et al. (1981: plagioclase). In addition, the ideal mixing model IlGkPy for ilmenite was applied. All pseudosections were calculated considering H_2O as a saturated component and Fe being only divalent. For metamorphic stage 1a (garnet core), the bulk-rock composition, obtained by XRF analyses and corrected for apatite by reducing CaO values according to the analyzed phosphorus content, was used to calculate the P-T pseudosection (sample MN14a, Fig. 6a; Table 6). For stage 1b (garnet mantle) an effective bulk-rock composition was applied by subtracting the garnet core from the bulk-rock composition, according to the following procedure: considering the garnet mode in the rock (20%) and the volume area of the core estimated from the X-ray maps (using the computer program ImageJ) and EMP analyses (around 40% in MN14A and MN40 samples, see Fig. 5), the garnet core volume relative to the bulk-rock was determined (6 vol%). Subsequently the average composition of the garnet core (based on EMP analysis) was calculated and then multiplied with 0.08, according to the

Please cite this article as: M. Scodina, G. Cruciani, M. Franceschelli, et al., Anticlockwise P-T evolution of amphibolites from NE Sardinia, Italy: Geodynamic implications for the..., Lithos, https://doi.org/10.1016/j.lithos.2018.12.003

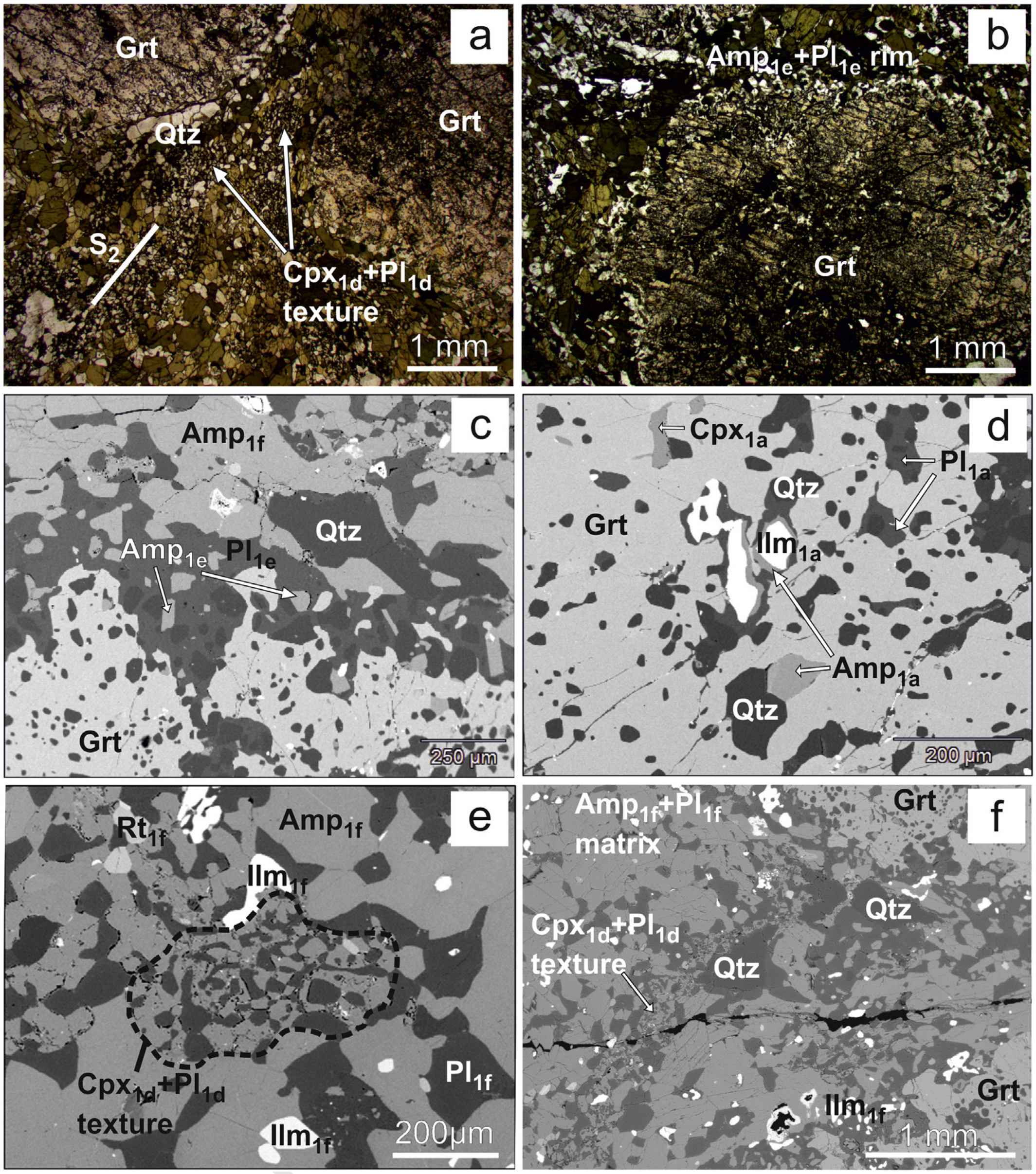

Fig. 4. Photomicrograph under plain polarized light and BSE images showing the relevant microstructures of garnet-bearing layers in amphibolites from Mt. Nieddu (Golfo Aranci area). (a) Clinopyroxene (Cpx) + plagioclase (Pl) flakes are stretched along the schistosity plane. Sample MN14A. (b) Overview of a garnet (Grt) porphyroblast rimmed by a Pl + amphibole (Amp) rim. Sample MN14A. (c) BSE image of the Pl + Amp rim around Grt; Amp can show compositional patch zoning. Sample MN40. (d) BSE image giving an overview of inclusions in Grt. Sample MN40. (e) BSE image of a Cpx + Pl symplectite. Sample MN14A. (f) BSE image giving an overview of Grt-bearing layers. Sample MN14A. Qtz = quartz; Chl = chlorite; Ilm = ilmenite; Rt = rutile.

higher density of garnet compared to the other minerals (plagioclase +amphibole) in the studied rocks. This composition was finally subtracted from the bulk composition used for stage 1a and then normalized to 100% (Table 6). The resulting P-T pseudosection is shown in Fig. 6c. For stage 1c (garnet rim) another effective bulk-rock composition was used after additional subtraction (12%) of the garnet mantle from the effective bulk-rock composition for stage 1b. The obtained P-T pseudosection for stage 1c is shown in Fig. 6e. All calculated P-T pseudosections were contoured by selected isopleths for contents of almandine, grossular, pyrope and spessartine in garnet.

Fig. 6b shows the intersections of almandine ($X_{Fe} = 0.56$), grossular ($X_{Ca} = 0.28$), pyrope ($X_{Mg} = 0.10$) and spessartine ($X_{Mn} = 0.07$) for the garnet core composition which occur at conditions of T = 680–720 °C and P = 0.8–1.0 GPa. These P-T conditions are compatible with $X_{Na} = 0.07$ of Cpx_{1a} and $X_{Ca} = 0.35$ of Pl_{1a} (see isopleths in Fig. 6b). The calculated mineral assemblage at T = 680–720 °C and P = 0.8–1.0 GPa is garnet + plagioclase + amphibole + clinopyroxene + ilmenite + biotite ± quartz; (Fig. 6a). Except for small amounts of biotite of 4 vol%, this assemblage matches the observed assemblage for stage 1a.

As manganese is adsorbed by garnet during prograde growth stages, it is not relevant for the calculation of the effective bulk-rock composition reaching the peak P-T conditions and during retrograde stages. Consequently, for defining the P-T conditions of stages 1b and 1c the spessartine isopleths were not considered because in the corresponding effective bulk-rock compositions the manganese contents are too low and, thus, not reliable. Fig. 6d shows the intersections of the isopleths for the molar fractions of grossular ($X_{Ca} = 0.27$), pyrope ($X_{Mg} = 0.10$) and almandine ($X_{Fe} = 0.59$) of the garnet mantle which occur at T = 680–730 °C and P = 1.0–1.2 GPa. The calculated mineral assemblage (garnet + plagioclase + amphibole + clinopyroxene + ilmenite + quartz + biotite ± rutile) at these P-T conditions is the same as for stage 1a except for the presence of rutile (Fig. 6c). This difference is

Please cite this article as: M. Scodina, G. Cruciani, M. Franceschelli, et al., Anticlockwise P-T evolution of amphibolites from NE Sardinia, Italy: Geodynamic implications for the..., Lithos, https://doi.org/10.1016/j.lithos.2018.12.003

Table 1
Representative microprobe analyses of core, mantle and rim of garnet grains from samples MN14A and MN40.

	MN14A			MN40		
	Core	Mantle	Rim	Core	Mantle	Rim
SiO_2	37.78	38.12	38.44	38.06	38.12	38.66
TiO_2	0.18	0.09	0.09	0.12	0.13	0.09
Al_2O_3	20.76	21.26	21.42	21.36	21.53	21.78
FeO	26.62	27.90	27.65	26.58	28.07	26.60
MnO	3.49	0.99	0.26	3.08	0.49	0.59
MgO	2.73	3.10	4.05	2.84	3.36	4.34
CaO	9.72	9.92	9.51	9.71	9.96	9.66
Total	101.28	101.38	101.42	101.75	101.66	101.72
oxygen	12	12	12	12	12	12
Si	2.98	2.98	2.99	2.97	2.97	2.98
Ti	0.01	0.01	0.01	0.01	0.01	0.01
Al	1.93	1.96	1.96	1.97	1.98	1.98
Fe^{2+}	1.75	1.83	1.80	1.74	1.83	1.72
Mn	0.23	0.07	0.02	0.20	0.03	0.04
Mg	0.32	0.36	0.47	0.33	0.39	0.50
Ca	0.82	0.83	0.79	0.81	0.83	0.80
Total	8.04	8.04	8.04	8.03	8.04	8.03
Alm	0.56	0.59	0.58	0.56	0.59	0.56
Prp	0.10	0.12	0.15	0.11	0.13	0.16
Grs	0.27	0.27	0.26	0.26	0.27	0.26
Sps	0.07	0.02	0.01	0.07	0.01	0.02

Table 3
Representative microprobe analyses of different textural varieties of clinopyroxene from samples MN14A and MN40.

	MN14A			MN40		
	Cpx1a	Cpx1d	Cpx1f	Cpx1a	Cpx1c	Cpx1d
SiO_2	52.71	52.41	52.95	50.96	51.60	52.37
TiO_2	0.20	0.25	0.12	0.30	0.15	0.17
Al_2O_3	3.32	1.53	1.45	2.66	1.79	1.81
FeO	10.93	8.88	9.67	12.06	11.35	9.32
MnO	0.00	0.08	0.20	0.08	0.09	0.06
MgO	12.00	13.01	12.49	11.01	11.74	12.72
CaO	19.79	23.26	22.79	21.86	22.17	23.08
Na_2O	0.86	0.60	0.68	0.86	22.17	0.68
Total	99.81	100.02	100.35	99.79	99.61	100.21
Oxygen	6	6	6	6	6	6
Si	1.97	1.96	1.98	1.93	1.94	1.96
Ti	0.01	0.01	0.00	0.01	0.00	0.01
Al	0.15	0.07	0.06	0.12	0.08	0.08
Fe^{2+}	0.34	0.28	0.30	0.38	0.36	0.29
Mn	0.00	0.00	0.01	0.00	0.00	0.00
Mg	0.67	0.73	0.70	0.62	0.66	0.71
Ca	0.79	0.93	0.91	0.89	0.89	0.93
Na	0.06	0.04	0.05	0.06	0.05	0.05
Total	3.99	4.02	4.01	4.01	3.99	4.03
X_{Na}	0.07	0.04	0.05	0.07	0.06	0.05
X_{Mg}	0.66	0.72	0.70	0.62	0.65	0.71

compatible with the appearance of rutile inclusions in the garnet mantle. Isopleths representing the garnet rim composition for grossular (X_{Ca} = 0.26), pyrope (X_{Mg} = 0.16) and almandine (X_{Fe} = 0.56; see Table 1 and Fig. 6f), intersect in two different P-T ranges: at HP granulite-facies (T = 690–730 °C and P = 1.3–1.4 GPa) and amphibole-eclogite facies (T = 600–640 °C and P = 1.8–2.0 GPa) conditions. However, it is unlikely that the studied rocks reached the amphibole-eclogite facies due to the occurrence of plagioclase at all stages of the metamorphic evolution (see Fig. 3). The calculated assemblage at T = 690–740 °C and P = 1.3–1.5 GPa (Fig. 6e) is clinopyroxene + plagioclase + amphibole + garnet + quartz + rutile + biotite. The occurrence of rutile (stage 1c) instead of ilmenite (stages 1a-b) is compatible with the observed minerals. The calculated garnet volume (see isomodes in Fig. 6f) at T = 690–740 °C and P = 1.3–1.5 GPa is around 30 vol% and compatible with the determined garnet mode.

In order to determine the conditions of stage 2, the bulk-rock composition of the host amphibolites (samples MN7 and MN8), obtained by XRF analysis and corrected for apatite, was used to calculate P-T pseudosections (Table 6). Fig. 6g and h show the result for sample MN7 and the intersection of isopleths for the Si content in Amp_2 (Si = 6.9 apfu) and X_{Ca} = 0.86 of Pl_2. The obtained conditions of 560–620 °C and 0.7–0.8 GPa refer to P-T fields of two assemblages which differ for the presence of quartz (clinopyroxene + plagioclase + amphibole + garnet + biotite + titanite ± quartz). Except for biotite + titanite (observed were chlorite + ilmenite), this assemblage for stage 2 was found.

Table 2
Representative microprobe analyses of different textural varieties of plagioclase from samples MN14A, MN40, MN7 and MN8.

SiO_2	60.80	65.01	64.15	59.90	60.64	61.33	46.21	46.14
TiO_2	0.01	0.01	0.01	0.00	0.00	0.00	0.01	–
Al_2O_3	25.09	21.75	22.53	25.04	24.59	24.10	33.49	33.36
FeO	0.36	0.16	0.14	0.50	0.23	0.21	0.09	0.03
MnO	0.05	0.01	0.00	0.04	0.02	0.00	–	–
CaO	6.91	3.19	4.02	6.97	6.49	5.85	17.26	17.53
Na_2O	7.21	9.46	9.10	8.03	8.01	8.55	1.59	1.59
K_2O	0.16	0.47	0.36	0.08	0.29	0.21	0.02	0.01
Total	100.59	100.06	100.31	100.56	100.27	100.25	98.66	98.65
Oxygen	8	8	8	8	8	8	8	8
Si	2.69	2.87	2.83	2.66	2.70	2.72	2.10	2.10
Ti	0.00	0.00	0.00	0.00	0.00	0.00	0.00	–
Al	1.31	1.13	1.17	1.31	1.29	1.26	1.79	1.78
Fe^{2+}	0.01	0.01	0.01	0.02	0.01	0.01	0.00	0.00
Mn	0.00	0.00	0.00	0.00	0.00	0.00	–	–
Ca	0.33	0.15	0.19	0.33	0.31	0.28	0.84	0.85
Na	0.62	0.81	0.78	0.69	0.69	0.74	0.14	0.14
K	0.01	0.03	0.02	0.01	0.02	0.01	0.00	0.00
Total	4.97	5.00	5.00	5.02	5.02	5.02	4.88	4.88
X_{Na}	0.65	0.84	0.80	0.68	0.69	0.73	0.14	0.14
X_{Ca}	0.35	0.16	0.20	0.32	0.31	0.27	0.86	0.86

5.2. Rutile thermometry

As quartz and zircon are present in the studied rocks, we applied the Zr-in-rutile thermometer. We used the calibration by Tomkins et al. (2007) because it considers, unlike the previous ones (Watson et al., 2006; Zack et al., 2004), a slight pressure dependence of the thermometer although it might slightly overestimate the formation temperatures for rutile in metabasites (Tomkins et al., 2007).

Fig. 7 shows a histogram for the temperatures obtained from the Zr-in-rutile thermometer on eighty-seven analyses of rutile (see Supplementary Table S1 of supplementary material for Zr contents and calculated temperatures) from the amphibolites at Mt. Nieddu. The pressures considered for the thermometric calculations on Rt_{1c} and Rt_{1f} are 1.4 GPa, reached at peak conditions during the growth of the garnet rim (see above), and 0.8 GPa, respectively.

Rt_{1c} records a limited range of temperatures (680–720 °C) with a peak of 700–710 °C which fits very well the temperature interval obtained with pseudosections for stage 1c. Temperatures recorded by Rt_{1f} are slightly lower (650–720 °C), with two peaks at 670–680 and 700 °C. This result suggests a slight decrease in temperature after the end of garnet growth during the decompression phase (see next paragraph) as registered also by the pseudosection modelling.

6. Discussion

6.1. P-T path of the Golfo Aranci amphibolites

The P-T path recorded by the zoning of garnet and the observed mineral assemblages in amphibolites from Mt. Nieddu is anticlockwise (Fig. 8). The reconstructed trajectory shows a remarkable increase in pressure (from 0.7 to 1.4 GPa) and a very slight increase in temperature during the prograde path. These results testify that the studied amphibolites reached their maximum pressure conditions in the HP granulite

Please cite this article as: M. Scodina, G. Cruciani, M. Franceschelli, et al., Anticlockwise P-T evolution of amphibolites from NE Sardinia, Italy: Geodynamic implications for the..., Lithos, https://doi.org/10.1016/j.lithos.2018.12.003

Table 4
Representative microprobe analysis of different textural varieties of amphibole from samples MN14A, MN40, MN7 and MN8. The H_2O content was calculated.

	MN14A			MN40				MN7	MN8
	Amp1d	Amp1f	Amp3	Amp1a	Amp1c	Amp1e	Amp1e	Amp2	Amp2
SiO_2	43.14	43.38	54.13	43.16	41.64	43.48	43.27	48.53	48.67
TiO_2	2.15	1.85	0.10	1.33	2.01	1.59	1.47	0.52	0.50
Al_2O_3	10.97	10.53	2.12	11.55	12.04	10.76	10.71	8.41	8.12
FeO	3.28	4.56	11.51	3.86	4.95	5.79	6.10	6.31	6.99
Fe_2O_3	14.14	14.09	1.68	14.07	14.89	13.41	13.79	4.51	3.69
MnO	0.09	0.09	0.05	0.00	0.08	0.03	0.08	0.13	0.19
MgO	10.87	10.48	15.45	10.79	9.05	9.77	9.91	15.60	15.78
CaO	11.80	11.58	12.85	11.69	11.64	11.35	11.39	12.17	12.64
Na_2O	1.88	1.80	0.21	1.64	1.91	1.86	1.64	1.24	1.15
K_2O	0.82	0.75	0.05	0.73	0.92	0.74	0.76	0.11	0.10
BaO	0.08	0.07	0.00	0.00	0.10	0.04	0.01	0.04	0.00
H_2O	2.07	2.06	2.10	2.07	2.05	2.04	2.05	2.10	2.10
Total	101.29	101.24	100.25	100.89	101.28	100.88	101.18	99.67	99.93
Oxygen	23	23	23	23	23	23	23	23	23
Si	6.24	6.31	7.74	6.26	6.10	6.35	6.32	6.94	6.95
Al^{IV}	1.76	1.69	0.26	1.74	1.90	1.65	1.68	1.06	1.04
Al^{VI}	0.12	0.11	0.10	0.24	0.18	0.21	0.16	0.36	0.32
Ti	0.23	0.20	0.01	0.15	0.22	0.17	0.16	0.06	0.05
Fe^{2+}	0.40	0.55	1.38	0.47	0.61	0.71	0.75	0.75	0.84
Fe^{3+}	1.54	1.54	0.18	1.54	1.64	1.47	1.52	0.49	0.40
Mn	0.01	0.01	0.01	0.00	0.01	0.00	0.01	0.02	0.02
Mg	2.35	2.27	3.30	2.33	1.98	2.13	2.16	3.33	3.36
Ca	1.83	1.80	1.97	1.82	1.83	1.78	1.78	1.87	1.94
Na	0.53	0.51	0.06	0.46	0.54	0.53	0.46	0.34	0.32
K	0.15	0.14	0.01	0.14	0.17	0.14	0.14	0.02	0.02
Ba	0.00	0.00	0.00	0.00	0.01	0.00	0.00	0.00	0.00
H	2.00	2.00	2.00	2.00	2.00	2.00	2.00	2.00	2.00
X_{Mg}	0.86	0.80	0.71	0.83	0.77	0.75	0.74	0.81	0.80
	tsch	tsch-hbl	act	tsch-hbl	tsch	tsch-hbl	tsch-hbl	Mg-hbl	Mg-hbl

facies at T = 690–740 °C and P = 1.3–1.5 GPa. As suggested by the isobaric position of the garnet isomodes (Fig. 6f), it is likely that garnet porphyroblasts stopped their growth after reaching the peak pressure. Afterwards a decompression event together with a slight temperature decrease (with the appearance of clinopyroxene+plagioclase symplectites, coronae and matrix in garnet-bearing layers) occurred at temperatures around 670–710 °C, as documented by the Zr content in rutile (Fig. 7). Subsequently, the amphibolites experienced massive overgrowth by green amphibole and plagioclase at amphibolite-facies conditions (T = 560–620 °C and P = 0.7–0.8 GPa) during further retrograde metamorphism. The late formation of epidote veins, chlorite and actinolite suggests the continuation of a retrograde evolution of these rocks towards the greenschist facies, as already documented for several metabasites from NE Sardinia (Cruciani et al., 2012, 2015b; Franceschelli et al., 2002, 2007), at conditions of about P = 0.2–0.3 GPa and T = 330–350 °C.

Table 5
Representative microprobe analysis of different textural varieties of chlorite, epidote and ilmenite from samples MN7, MN8 and MN40.

	MN7		MN8		MN40	
	Chl	Ep	Ep	Ep	Ilm1a	Ilm1f
SiO_2	29.40	37.84	38.73	38.74	–	–
TiO_2	0.01	0.05	0.10	0.13	47.96	50.70
Al_2O_3	24.23	27.96	27.18	29.88	–	–
FeO	10.65	6.42	7.86	3.81	49.24	47.73
MnO	0.20	0.08	0.10	0.03	1.01	0.33
MgO	22.18	0.06	0.08	0.24	0.05	0.04
CaO	0.31	24.02	24.11	24.23	0.06	0.07
Na_2O	0.04	–	–	–	–	–
K_2O	0.03	0.02	–	0.01	–	–
H_2O	12.98	3.55	1.85	2.93	–	–
Total	100.03	100.00	100.00	100.00	98.31	98.92
oxygen	28	12.5	12.5	12.5	3	3
Si	5.73	2.97	2.99	2.99	–	–
Ti	0.00	0.00	0.00	0.01	0.92	0.97
Al	11.56	2.59	2.48	2.72	–	–
Fe^{2+}	1.73	–	–	–	0.90	0.96
Fe^{3+}	–	0.42	0.50	0.25	0.15	0.05
Mn^{2+}	0.03	–	–	–	0.02	0.01
Mn^{3+}	–	0.01	0.01	0.00	–	–
Mg	6.44	0.01	0.01	0.03	0.00	0.00
Ca	0.00	2.02	2.00	2.01	0.00	0.00
Na	0.00	–	–	–	–	–
K	0.00	–	–	–	–	–
Total	25.49	8.02	7.99	8.01	1.99	1.99

We compared our P-T modelling with that of retrogressed eclogite lenses in the Golfo Aranci area (Fig. 8). Cruciani et al. (2018) described the early metamorphic evolution of kyanite-bearing eclogites by modelling their garnet zoning. These rocks underwent a clockwise P-T path with the following conditions (Fig. 8): T = 580–630 °C and P = 1.6–2.0 GPa for the garnet core, T = 620–690 °C and P = 2.0–2.2 GPa for the garnet mantle, and T = 650–700 °C and P = 1.4–1.9 GPa for the garnet rim. This trajectory is similar to those of other eclogites from NE Sardinia (Cruciani et al., 2011; Giacomini et al., 2005a) and quite different from the amphibolites presented in this work. However, the P-T conditions recorded by the garnet rim in both eclogites and studied rocks converge in the P-T range between amphibole facies, eclogite facies, and HP granulite facies at P = 1.4–1.6 GPa and T = 680–720 °C. Thus, it is likely that eclogites and amphibolites experienced a similar decompression/exhumation path (see next paragraph) from the HP amphibolite facies on.

Franceschelli et al. (2002) determined the P-T conditions of adjacent ultrabasic amphibolites based on coronitic microstructures around olivine and plagioclase using conventional geothermobarometry. The recorded granulite-facies and amphibolite-facies conditions are T = 700–750 °C at P = 0.8–1.0 GPa and T = 560–650 °C at P = 0.4–0.6 GPa, respectively. Considering the proximity between the ultrabasic amphibolites studied by Franceschelli et al. (2002) and the here studied amphibolites (these are separated only by a tectonic contact) we can assume that, after an early decompression phase, both rock types were brought together and followed the same retrograde path during further exhumation.

Please cite this article as: M. Scodina, G. Cruciani, M. Franceschelli, et al., Anticlockwise P-T evolution of amphibolites from NE Sardinia, Italy: Geodynamic implications for the..., Lithos, https://doi.org/10.1016/j.lithos.2018.12.003

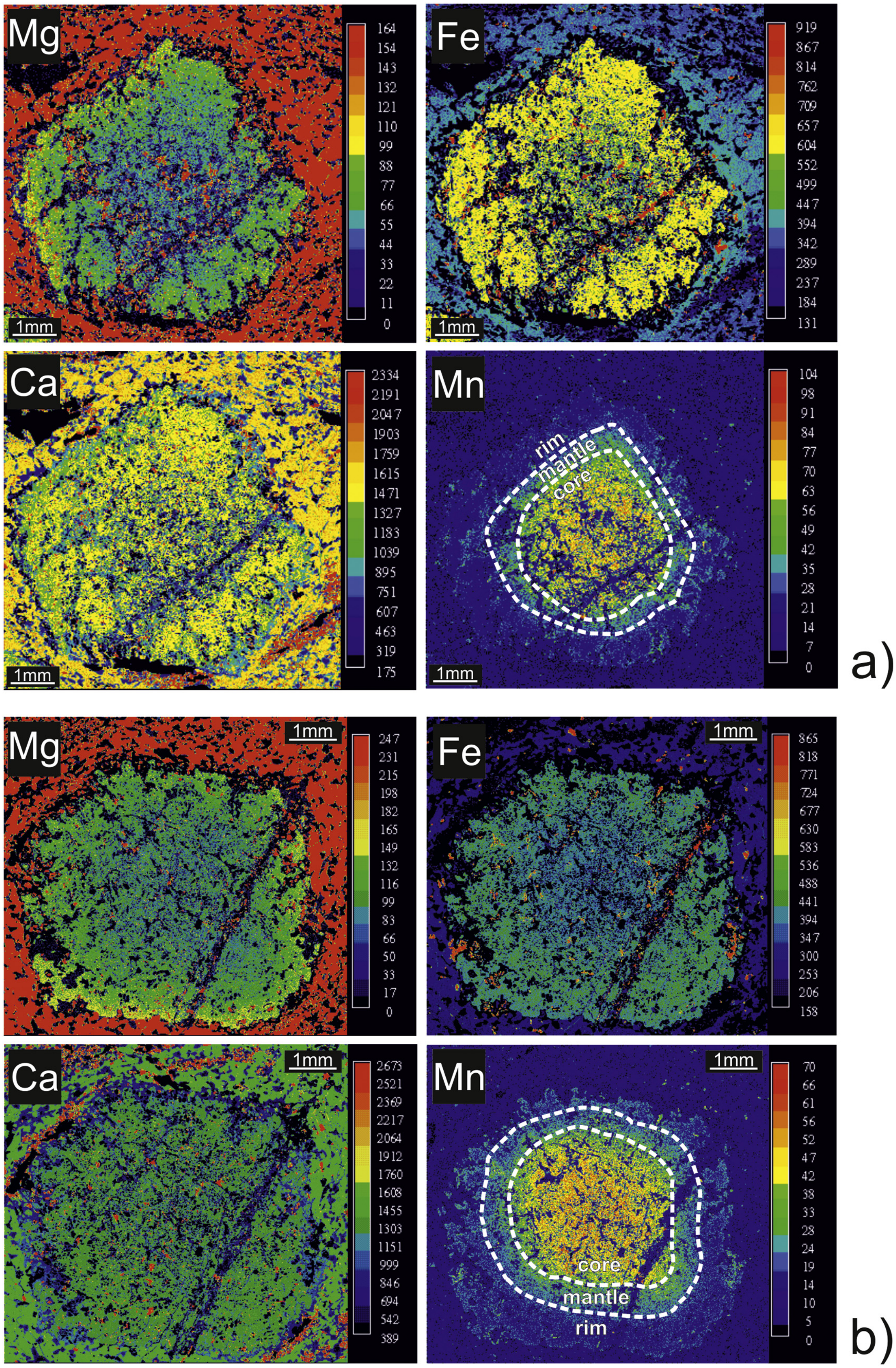

Fig. 5. (a) Mg, Fe, Ca and Mn concentration maps of a selected garnet grain from sample MN14A. (b) Mg, Fe, Ca and Mn concentration maps of a selected garnet grain from sample MN40. The scales for the colour code on the right-hand side of each image indicate counts of specific X-ray radiation per time unit.

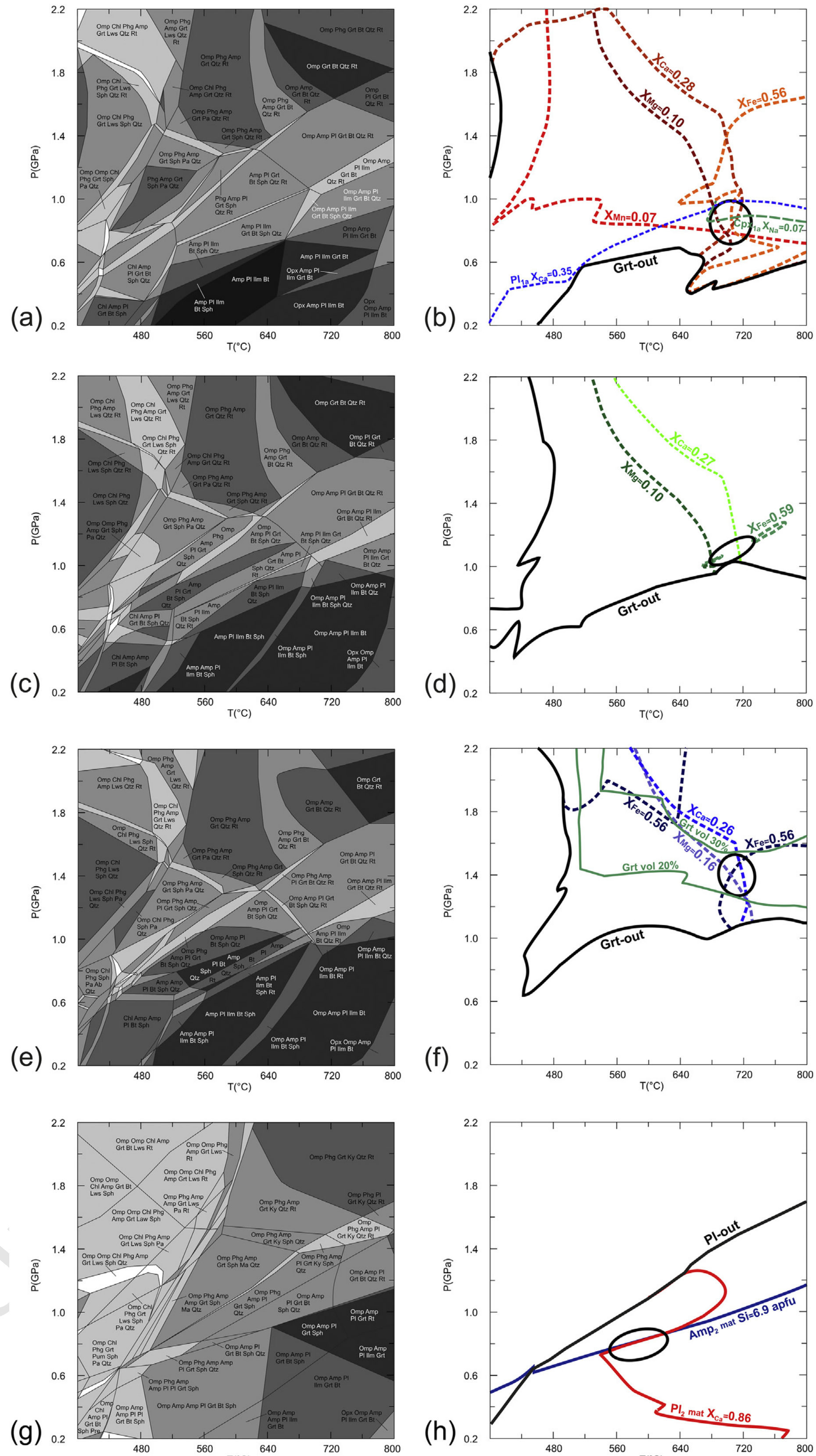

Fig. 6. (a) P-T pseudosection calculated in the NCKFMASH+Ti + Mn system for the bulk rock composition of sample MN14A (bulk core in Table 6). (b) Estimated P-T conditions for the growth of the garnet core. Dashed green line = X_{Na} in clinopyroxene inclusion in garnet core; blue dashed line = X_{Ca} in plagioclase inclusion in garnet core (c) P-T pseudosection calculated in the NCKFMASH+Ti + Mn system for the composition of sample MN14A minus garnet core (bulk mantle in Table 6). (d) Estimated P-T conditions for the growth of the garnet mantle. (e) P-T pseudosection calculated in the NCKFMASH+Ti + Mn system for the composition of sample MN14A minus garnet core and mantle (bulk rim in Table 6). (f) Estimated P-T conditions for the growth of the garnet rim. Green bold lines = isomodes for garnet. (g) P-T pseudosection calculated in the NCKFMASH+Ti + Mn system for sample MN7. (h) Estimated P-T conditions for the growth of the matrix minerals in the studied rock. (For interpretation of the references to colour in this figure legend, the reader is referred to the web version of this article.)

Table 6
Bulk rock analyses (wt%) of samples MN7, MN8, MN14A and MN40 determined by X-ray fluorescence spectrometry (XRF) and modified compositions for the calculation of P-T pseudosections. "Bulk mantle" and "bulk rim" compositions are determined by subtracting the garnet core and core+mantle of garnet, respectively, from the bulk-rock composition (see text for details).

	MN14A				MN40				MN7		MN8	
	Bulk XRF	Bulk core	Bulk mantle	Bulk rim	Bulk XRF	Bulk core	Bulk mantle	Bulk rim	Bulk XRF	Bulk rock	Bulk XRF	Bulk rock
SiO_2	47.39	49.75	51.43	52.46	49.20	49.77	51.50	52.67	48.68	49.59	47.68	48.52
TiO_2	2.48	2.60	2.96	3.19	2.55	2.58	2.93	3.17	0.23	0.24	0.25	0.26
Al_2O_3	13.41	14.07	13.04	12.39	13.94	14.10	13.05	12.43	17.70	18.03	18.82	19.15
Fe_2O_3	13.29	–	–	–	13.64	–	–	–	6.25	–	6.59	–
FeO_{tot}	–	12.55	10.47	9.13	–	12.42	10.27	8.87	–	5.73	–	6.04
MgO	6.63	6.96	7.58	7.96	6.97	7.05	7.66	8.03	9.39	9.57	8.62	8.77
MnO	0.14	0.15	0.03	0.01	0.14	0.14	0.03	0.01	0.11	0.11	0.10	0.11
CaO	9.89	10.01	10.00	10.04	10.23	9.98	10.00	10.01	14.84	15.11	15.25	15.51
Na_2O	2.92	3.06	3.52	3.79	3.10	3.13	3.60	3.88	1.50	1.53	1.45	1.47
K_2O	0.54	0.56	0.65	0.70	0.55	0.55	0.63	0.58	0.08	0.08	0.15	0.16
P_2O_5	0.27	–	–	–	0.28	–	–	–	0.01	–	0.01	–

6.2. Geodynamic scenario

We explain the difference of the metamorphic evolution (clockwise versus anticlockwise P-T path) shown by the eclogites and amphibolites (former granulites) in the light of the geodynamic scenario recently proposed by Massonne et al. (2018) for southern Corsica and northern Sardinia. Both regions, geographically separated by an only 12 km wide sea channel, show similar age relations and tectonic structures. For example, the age of magmatic protoliths of the Zicavo and Porto-Vecchio orthogneiss, constrained by U—Pb method on zircon at 458 ± 32 Ma and 465 + 19/−16 Ma (Faure et al., 2014 and references therein) are close to the ages of similar augen gneiss of Sardinia (Lodè orthogneiss, 456 ± 14 Ma, Helbing and Tiepolo, 2005). Dating of zircon from Golfo Aranci eclogites, embedded within the HGMC, by Giacomini et al. (2005a,b) resulted in ages of 460 ± 5 Ma for igneous domains, whereas metamorphic ages clustered around Early Visean (~345 Ma) and between Late Visean (~325 Ma) and 300 Ma. The older cluster was related to the HP eclogite event and the younger one to post-HP amphibolite-facies equilibration. In southern Corsica, the HP granulite-facies metamorphism has been dated at 360 Ma by Giacomini et al. (2008). This age was confirmed by Li et al. (2014a) and is, thus, likely also for the HP granulite-facies metamorphism in northern Sardinia studied here. The HP metamorphic occurrences are also similar in northern Sardinia and southern Corsica. In north-eastern Sardinia HP metamorphic conditions are testified by eclogite bodies (Cortesogno et al., 2004; Cruciani et al., 2011, 2012, 2015a; Franceschelli et al., 2007; Giacomini et al., 2005a), gneisses and migmatites which experienced pressures >1 GPa (Cruciani et al., 2008; Massonne et al., 2013), and micaschists with peak P-T conditions up to 1.8 GPa (Cruciani et al., 2013). These rocks might have their northern counterpart in the south-eastern Corsica granulites that underwent pressures as high as 1.9 GPa (Giacomini et al., 2008).

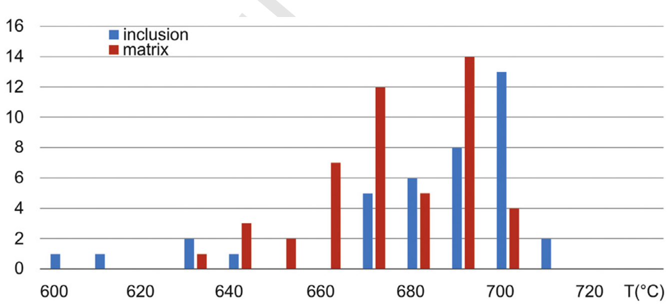

Fig. 7. Histogram showing the temperature results applying the Zr-in-rutile thermometer of Tomkins et al. (2007) on eighty-seven analyses of rutile (rutile inclusions in garnet porphyroblasts are represented in blue and rutile grains in the matrix of the layers in red) from samples MN14A and MN40. (For interpretation of the references to colour in this figure legend, the reader is referred to the web version of this article.)

The metamorphic evolution of the amphibolites of the Golfo Aranci area took place during and after the continental collision between the peri-Gondwanian terranes (previously accreted to Laurussia) and Gondwana, after the closure of the South-Armorican ocean, a branch of the Rheic ocean, in the late Devonian (Rossi et al., 2009), before 360 Ma (Giacomini et al., 2008). The continental collision event, which caused crustal thickening, resulted in a HP migmatization (Massonne et al., 2013) and a Barrovian-type metamorphism (Ricci et al., 2004) in the Inner Zone of the Sardinian Variscan basement.

The anticlockwise metamorphic P-T path presented in this work is quite different from the typical clockwise paths (Fig. 8) reconstructed for several metabasites and HP migmatites of NE Sardinia and it deserves some further geodynamic considerations. Anticlockwise P-T paths are not common in the literature of subduction-collisional mountain belts but several studies confirmed them (Duan et al., 2017; Groppo and Rolfo, 2008; Li et al., 2014b; Li et al., 2017; Pitra and Guiraud, 1996; Vignaroli et al., 2005; Waizenhöfer and Massonne, 2017; Xiang et al., 2012). Considering the metamorphic rocks from the Corsica-Sardinia block, the only hitherto documented anticlockwise P-T path is that described by Massonne et al. (2018). These authors reconstructed the P-T-t evolution of garnet-bearing micaschists from the area of Porto

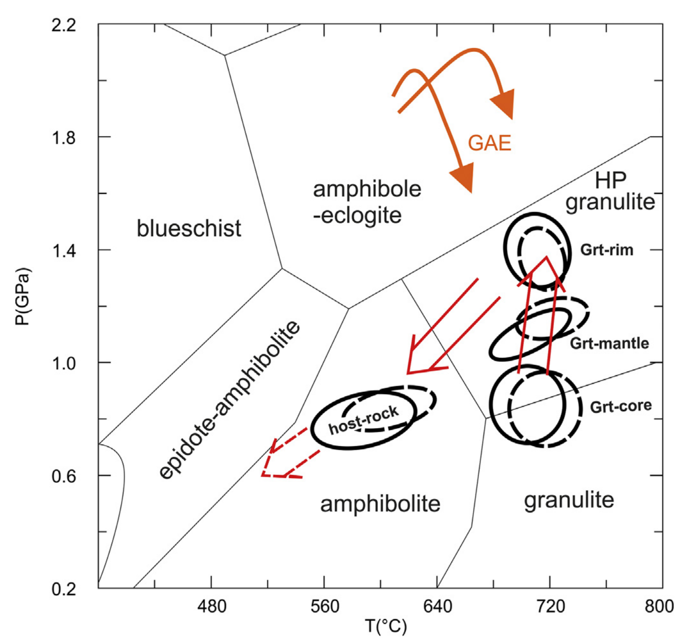

Fig. 8. P-T path of the studied amphibolites from the Golfo Aranci area (sample MN14A and MN7, bold black ellipses and sample MN40 and MN8, dashed ellipses) compared to eclogites from the same area. GAE = Golfo Aranci eclogite (from Cruciani et al., 2018). Facies field areas from Liou et al. (1998).

Vecchio, south-eastern Corsica. These rocks reached peak conditions at P = 0.7 GPa and T = 600–630 °C, which are lower than those determined for coeval migmatitic gneisses (peak pressure: 1.0–1.2 GPa, Cruciani et al., 2008; Massonne et al., 2013) and micaschist (1.8 GPa, Cruciani et al., 2013) from NE Sardinia. Massonne et al. (2018) interpreted the rocks with anticlockwise path and low peak pressure as part of the upper plate in the continent-continent collisional scenario, whereas the contemporaneous metamorphic HP rocks from NE Sardinia were part of the lower plate. Both, micaschists from Corsica and HP rocks from NE Sardinia, were subsequently involved in an exhumation channel (see Massonne, 2016b for definitions and further explanation), where rock slices from different crustal levels of both upper and lower continental plates were brought adjacent to each other very likely in Visean times. Probably most of the material in the exhumation channel is from the upper portion of the downgoing continental plate and thus relatively cold. Hotter slices of the overlying continental plate, which are involved in the exhumation channel, are cooled down by this material still at depths where the separation of such slices from the upper continental plate occurs. Thus, these rock slices experienced an anticlockwise P-T path.

This model is suitable to explain the P-T path of the amphibolites studied here. The difference of the peak pressure conditions between the micaschists reported by Massonne et al. (2018) and the here studied rocks is the result of a greater depth reached by our rocks and, thus, a different position of them between the colliding plates (Fig. 9). Perhaps this could be also related to their different protolith nature (basic-ultrabasic versus sedimentary). According to the considered geotectonic model, the recorded tectono-metamorphic evolution of the studied amphibolites began in the Upper Devonian during subduction of oceanic crust under the peri-Gondwanan terrane which was previously accreted to Laurussia. These rocks were located probably in the hot, lowermost part of the upper plate, adjacent to the subducting slab, at depths around 35 km (0.8–0.9 GPa; Fig. 9a), whereas the eclogites from the Golfo Aranci area were part of the relatively cold subducting

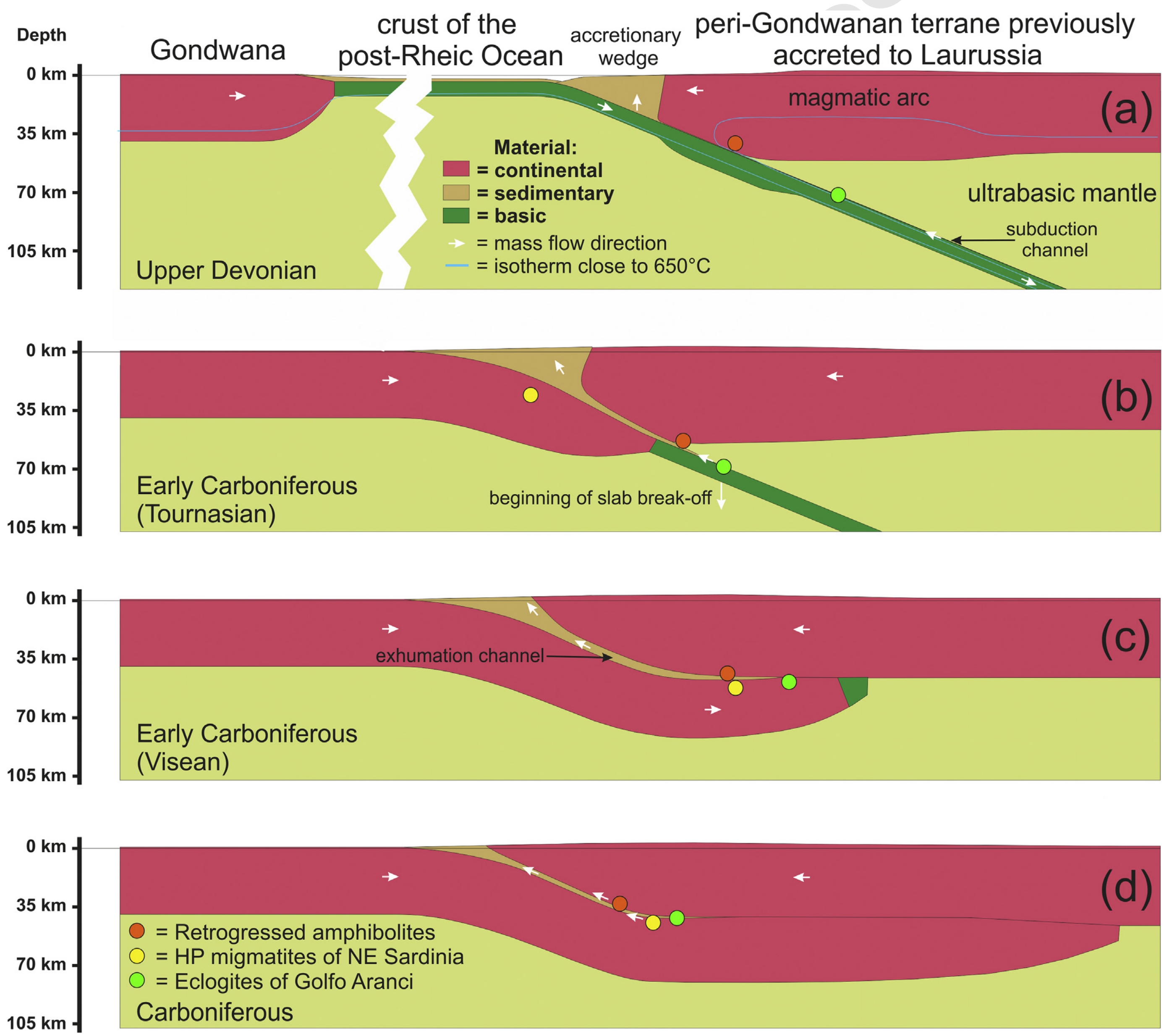

Fig. 9. Sketch of the geodynamic evolution of the studied amphibolites from the Golfo Aranci area during the Variscan orogeny (modified after Massonne et al., 2018). (a) Subduction of oceanic crust under the Laurussia plate and the peri-Gondwanan terranes; (b) Continental collision and slab break-off event; (c) Crustal thickening and beginning of the particle path in the exhumation channel shown by a white arrow; (d) Exhumation of now adjacent amphibolites (red dots), HP migmatites (yellow dots), and eclogites from the Golfo Aranci area (green dots, Cruciani et al., 2018) in the exhumation channel. (For interpretation of the references to colour in this figure legend, the reader is referred to the web version of this article.)

Please cite this article as: M. Scodina, G. Cruciani, M. Franceschelli, et al., Anticlockwise P-T evolution of amphibolites from NE Sardinia, Italy: Geodynamic implications for the..., Lithos, https://doi.org/10.1016/j.lithos.2018.12.003

crust and reached greater depths (2.0–2.2 GPa, Cruciani et al., 2018). The amphibolites were buried to depths of 50–55 km (1.4 GPa) either by attachment (tectonic or subduction erosion) to the subducting oceanic crust or (less likely) by thickening of the upper plate during the Gondwana-Laurussia collision which occurred at the beginning of the Carboniferous. After the continental collision, the oceanic crust linked to Gondwana was involved in a break-off event (Fig. 9b) which is a common scenario invoked by many authors of recent studies of early Variscan rocks (Casini et al., 2015; Giacomini et al., 2008; von Raumer et al., 2014). However, some slices of oceanic crust, turned to eclogite, were exhumed in the subduction channel and then attached to the downgoing continental plate and the exhumation channel just before the break-off event occurred.

Subsequently, after a significant thrusting of Gondwana under Laurussia, around 345 Ma (Massonne et al., 2018), metamorphic rocks from both upper and lower plates were involved in a particle path (with an important strike-slip component according to Giacomini et al., 2008) in the above invoked exhumation channel (Fig. 9c). This tectonic event is characteristic of collisional belt settings, and typical also for active collisional chains like the Himalayas (Catlos et al., 2001; Iaccarino et al., 2015, 2017). The studied amphibolites as well as rocks from the uppermost part of the lower plate (the HP migmatites from NE Sardinia) and eclogites derived from the oceanic crust (Cruciani et al., 2018) were involved in this event. All these rocks were brought together and tectonically mixed within the exhumation channel during lower and middle Carboniferous times, probably starting in the Visean (Fig. 9d).

7. Concluding remarks

We reconstructed the early metamorphic evolution of amphibolite from the Migmatite Complex of NE Sardinia through thermodynamic modelling using P–T pseudosections. These rocks underwent a nearly isothermal burial path recorded by the compositional zoning in garnet. The estimated P–T conditions are 0.8–1.0 GPa and 680–720 °C for the formation of the garnet core, 1.0–1.2 GPa and 690–730 °C for the garnet mantle, and 1.3–1.4 GPa and 690–730 °C for the garnet rim. Thus, the amphibolites reached their peak conditions in the HP-granulite facies (according to the scheme of Liou et al., 1998) where the garnet growth ended and decompression began. Subsequently, the Golfo Aranci amphibolites experienced retrograde amphibolite- (at T = 560–620 °C and P = 0.7–0.8 GPa) and greenschist-facies conditions. As cooling occurred already during the early retrogression, an anti-clockwise P-T path resulted.

The metamorphic evolution of the amphibolites is related to a continental collision during the Variscan orogeny. The studied rocks, located in a lowermost section of the upper plate, were brought to depths of 50–55 km either by tectonic erosion or crustal thickening and subsequently exhumed along a particle path (probably with a significant strike-slip component) that involved continental slices from both upper and lower plates in an exhumation channel.

Supplementary data to this article can be found online at https://doi.org/10.1016/j.lithos.2018.12.003.

Acknowledgements

An anonymous reviewer and R. Cirrincione (University of Catania) are acknowledged for their helpful comments that improved the manuscript. The authors also wish to thank T. Theye who supported the EMP work at Universität Stuttgart. Financial support from FdS RAS F72F16003080002 and University of Cagliari funds is acknowledged. This work is part of the first author's Ph.D. thesis funded by Sardinia Regional Government (P.O.R. Sardegna F.S.E. Programme of the Autonomous Region of Sardinia, European Social Fund 2007-2013 - Axis IV Human Resources, Objective l.3, Line of Activity l.3.1).

References

Barca, S., Carmignani, L., Eltrudis, A., Franceschelli, M., 1995. Origin and evolution of the Permian-Carboniferous basin of Mulargia Lake (South-Central Sardinia, Italy) related to the Late-Hercynian extensional tectonic. Comptes Rendus de l'Académie des Sciences Paris 321 (IIa), 171–178.

Brandelik, A., 2009. CALCMIN – an EXCEL™ Visual basic application for calculating mineral structural formulae from electron microprobe analyses. Computers & Geosciences 35, 1540–1551.

Cappelli, B., Carmignani, L., Castorina, F., Di Pisa, A., Oggiano, G., Petrini, R., 1992. A Variscan suture zone in Sardinia: geological, geochemical evidence, Paleozoic Orogenies in Europe (special issue). Geodinamica Acta 5 (1–2), 101–118.

Carmignani, L., Carosi, R., Di Pisa, A., Gattiglio, M., Musumeci, G., Oggiano, G., Pertusati, P.C., 1994. The hercynian Chain in Sardinia (Italy). Geodinamica Acta 7, 31–47.

Carmignani, L., Oggiano, G., Barca, S., Conti, P., Eltrudis, A., Funedda, A., Pasci, S., Salvadori, I., 2001. Geologia della Sardegna. Note illustrative della Carta Geologica della Sardegna in scala 1:200,000. Memorie descrittive della Carta Geologica d'Italia LX 283.

Carosi, R., Oggiano, G., 2002. Structural evolution of Nord eastern Sardinia: insight on the tectonic evolution of the Variscan Belt. Comptes Rendus de l'Académie des. Sciences Paris 334, 287–294.

Carosi, R., Palmeri, R., 2002. Orogen parallel tectonic transport in the Variscan belt of northeastern Sardinia (Italy): implications for the exhumation of medium-pressure metamorphic rocks. Geological Magazine 139 (5), 497–511.

Carosi, R., Di Pisa, A., Iacopini, D., Montomoli, C., Oggiano, G., 2004. The structural evolution of the Asinara Island (NW Sardinia, Italy). Geodinamica Acta 17 (5), 309–329.

Carosi, R., Frassi, C., Iacopini, D., Montomoli, C., 2005. Post collisional transpressive tectonics in northern Sardinia (Italy). Journal of the Virtual Explorer 19 (paper 3).

Carosi, R., Frassi, C., Montomoli, C., 2009. Deformation during exhumation of medium- and high-grade metamorphic rocks in the Variscan chain in northern Sardinia (Italy). Geological Journal 44, 280–305.

Casini, L., Cuccuru, S., Maino, M., Oggiano, G., Tiepolo, M., 2012. Emplacement of the Arzachena Pluton (Corsica-Sardinia Batholith) and the geodynamics of incoming Pangaea. Tectonophysics 544–545, 31–49.

Casini, L., Cuccuru, S., Puccini, A., Oggiano, G., Rossi, P., 2015. Evolution of the Corsica-Sardinia Batholith and late-orogenic shearing of the Variscides. Tectonophysics 646, 65–78.

Castorina, F., Cesaraccio, G., Di Pisa, A., Oggiano, G., 1996. The amphibolitic stratified complex of Punta Scorno (Asinara Island, Sardinia, Italy): petrogenesis and tectonic interpretation. Plinius 16, 68–70.

Catlos, E.J., Harrison, T.M., Kohn, M.J., Grove, M., Ryerson, F.J., Manning, C.E., Upreti, B.N., 2001. Geochronologic and thermobarometric constraints on the evolution of the Main Central Thrust, Central Nepal Himalaya. Journal of Geophysical Research 106, 16177–16204.

Connolly, J.A.D., 1990. Multivariable phase diagrams: an algorithm based on generalized thermodynamics. American Journal of Science 290, 666–718.

Connolly, J.A.D., 2009. The geodynamic equation of state: what and how. Geochemistry, Geophysics, Geosystems 10, Q10014.

Connolly, J.A.D., Memmi, I., Trommsdorff, V., Franceschelli, M., Ricci, C.A., 1994. Forward modeling of calc-silicate microinclusions and fluid evolution in a graphitic metapelite, Northeast Sardinia. American Mineralogist 79, 960–972.

Cortesogno, L., Gaggero, L., Oggiano, G., Paquette, J.L., 2004. Different tectono-thermal evolutionary paths in eclogitic rocks from the axial zone of the Variscan chain in Sardinia (Italy) compared with the Ligurian Alps. Ofioliti 29, 125–144.

Cruciani, G., Franceschelli, M., Marchi, M., Zucca, M., 2002. Geochemistry of metabasite from NE Sardinia, Italy: nature of protoliths, magmatic trend, and geotectonic setting. Mineralogy and Petrology 74, 25–47.

Cruciani, G., Franceschelli, M., Jung, S., Puxeddu, M., Utzeri, D., 2008. Amphibole-bearing migmatites from the Variscan Belt of NE Sardinia, Italy: Partial melting of mid-Ordovician igneous sources. Lithos 105, 208–224.

Cruciani, G., Dini, A., Franceschelli, M., Puxeddu, M., Utzeri, D., 2010. Metabasite from the Variscan belt in NE Sardinia, Italy: within-plate OIB-like melts with very high Sr and low Nd isotope ratios. European Journal of Mineralogy 22, 509–523.

Cruciani, G., Franceschelli, M., Groppo, C., 2011. P-T evolution of eclogite-facies metabasite from NE Sardinia, Italy: insights into the prograde evolution of Variscan eclogites. Lithos 121, 135–150.

Cruciani, G., Franceschelli, M., Groppo, C., Spano, M.E., 2012. Metamorphic evolution of non-equilibrated granulitized eclogite from Punta de li Tulchi (Variscan Sardinia) determined through texturally controlled thermodynamic modeling. Journal of Metamorphic Geology 30, 667–685.

Cruciani, G., Franceschelli, M., Massonne, H.-J., Carosi, R., Montomoli, C., 2013. Pressure–temperature and deformational evolution of high-pressure metapelites from Variscan NE Sardinia, Italy. Lithos 175-176, 272–284.

Cruciani, G., Fancello, D., Franceschelli, M., Scodina, M., Spano, M.E., 2014a. Geothermobarometry of Al-silicate bearing migmatites from the Variscan chain of NE Sardinia, Italy: a P-T pseudosection approach. Periodico di Mineralogia 83 (1), 19–40.

Cruciani, G., Franceschelli, M., Foley, S.F., Jacob, D.E., 2014b. Anatectic amphibole and restitic garnet in Variscan migmatite from NE Sardinia, Italy: insights into partial melting from mineral trace elements. European Journal of Mineralogy 26 (3), 381–395.

Cruciani, G., Franceschelli, M., Groppo, C., Oggiano, G., Spano, M.E., 2015a. Re-equilibration history and P-T path of eclogites from Variscan Sardinia, Italy: a case study from the medium-grade metamorphic complex. International Journal of Earth Sciences 104, 797–814.

Cruciani, G., Montomoli, C., Carosi, R., Franceschelli, M., Puxeddu, M., 2015b. Continental collision from two perspectives: a review of Variscan metamorphism and deformation in northern Sardinia. Periodico di Mineralogia 84, 657–699.

Cruciani, G., Franceschelli, M., Scodina, M., Puxeddu, M., 2018. Garnet zoning in kyanite-bearing eclogite from Golfo Aranci: new data on the early prograde P-T evolution in NE Sardinia, Italy. Geological Journal https://doi.org/10.1002/gj.3169.

Dale, J., Powell, R., White, R.W., Elmer, F.L., Holland, J.B., 2005. A thermodynamic model for Ca–Na clinoamphiboles in Na_2O–CaO–FeO–MgO–Al_2O_3–SiO_2–H_2O–O for petrological calculations. Journal of Metamorphic Geology 23, 771–791.

Di Vincenzo, G., Carosi, R., Palmeri, R., 2004. The relationship between tectono-metamorphic evolution and argon isotope records in white mica: constraints from in situ ^{40}Ar-^{39}Ar laser analysis of the Variscan basement of Sardinia. Journal of Petrology 45, 1013–1043.

Duan, Z., Wei, C., Rehman, H.U., 2017. Metamorphic evolution and zircon ages of pelitic granulites in eastern Hebei, North China Craton: insights into the regional Archean P–T–t history. Precambrian Research 292, 240–257.

Faure, M., Rossi, P., Gaché, J., Melleton, J., Frei, D., Li, X., Lin, W., 2014. Variscan orogeny in Corsica: new structural and geochronological insights, and its place in the Variscan geodynamic framework. International Journal of Earth Sciences 103, 1533–1551.

Franceschelli, M., Memmi, I., Ricci, C.A., 1982. Ca distribution between garnet and plagioclase in pelitic and psammitic schists from the metamorphic basement of North-Eastern Sardinia. Contributions to Mineralogy and Petrology 80, 285–295.

Franceschelli, M., Eltrudis, A., Memmi, I., Palmeri, R., Carcangiu, G., 1998. Multi-stage metamorphic re-equilibration in eclogitic rocks from the Hercynian basement of NE Sardinia (Italy). Mineralogy and Petrology 62, 167–193.

Franceschelli, M., Carcangiu, G., Caredda, A.M., Cruciani, G., Memmi, I., Zucca, M., 2002. Transformation of cumulate mafic rocks to granulite and re-equilibration in amphibolite and greenschist facies in NE Sardinia, Italy. Lithos 63, 1–18.

Franceschelli, M., Puxeddu, M., Cruciani, G., 2005a. Variscan metamorphism in Sardinia, Italy: review and discussion. Journal of the Virtual Explorer 19 (paper 2).

Franceschelli, M., Puxeddu, M., Cruciani, G., Dini, A., Loi, M., 2005b. Layered amphibolite sequence in NE Sardinia, Italy: remnant of a pre-Variscan mafic-silicic layered intrusion? Contributions to Mineralogy and Petrology 149, 164–180.

Franceschelli, M., Puxeddu, M., Cruciani, G., Utzeri, D., 2007. Metabasites with eclogite facies relics from Variscides in Sardinia, Italy: a review. International Journal of Earth Sciences 96, 795–815.

Ghezzo, C., Memmi, I., Ricci, C.A., 1979. Un evento granulitico nel basamento metamorfico della Sardegna nordorientale. Memorie della Societa Geologica Italiana 20, 23–38.

Giacomini, F., Bomparola, R.M., Ghezzo, C., 2005a. Petrology and geochronology of metabasites with eclogite facies relics from NE Sardinia: constraints for the Palaeozoic evolution of Southern Europe. Lithos 82, 221–248.

Giacomini, F., Bomparola, R.M., Ghezzo, C., 2005b. The pre-Variscan magmatic-sedimentary history in the high-grade metamorphic basement of northern Sardinia (Italy): constraints from U/Pb geochronology and geochemistry. Epitome. Geoitalia, Quinto Forum Italiano di Scienze della Terra. Spoleto 21–23 (September 2005).

Giacomini, F., Bomparola, R.M., Ghezzo, C., Guldbransen, H., 2006. The geodynamic evolution of the southern European Variscides: constraints from the U/Pb geochronology and geochemistry of the lower Paleozoic magmatic-sedimentary sequences of Sardinia (Italy). Contributions to Mineralogy and Petrology 152, 19–42.

Giacomini, F., Dallai, L., Carminati, E., Tiepolo, M., Ghezzo, C., 2008. Exhumation of a Variscan orogenic complex: insights into the composite granulitic–amphibolitic metamorphic basement of Southeast Corsica (France). Journal of Metamorphic Geology 26, 403–436.

Green, E.C.R., Holland, T.J.B., Powell, R., 2007. An order-disorder model for omphacitic pyroxenes in the system jadeite-diopside-hedenbergite-acmite with applications to eclogitic rocks. American Mineralogist 92, 1181–1189.

Groppo, C., Rolfo, F., 2008. Counterclockwise P-T evolution of the Aghil Range: metamorphic record of an accretionary melange between Kunlun and Karakorum (SW Sinkiang, China). Lithos 105, 365–378.

Helbing, H., Tiepolo, M., 2005. Age determination of Ordovician magmatism in NE Sardinia and its bearing on Variscan basement evolution. Journal of the Geological Society of London 162, 689–700.

Helbing, H., Frisch, W., Bons, P.D., 2006. South Variscan terrane accretion: Sardinian constraints on the intra-Alpine Variscides. Journal of Structural Geology 28, 1277–1291.

Holland, T.J.B., Powell, R., 1996. Thermodynamics of order-disorder in minerals, 2. Symmetric formalism applied to solid solutions. American Mineralogist 81, 1425–1437.

Holland, T.J.B., Powell, R., 1998. An internally consistent thermodynamic data set for phases of petrological interest. Journal of Metamorphic Geology 16, 309–343.

Holland, T.J.B., Baker, J.M., Powell, R., 1998. Mixing properties and activity-composition relationships of chlorites in the system MgO–FeO–Al_2O_3–SiO_2–H_2O. European Journal of Mineralogy 10, 395–406.

Iaccarino, S., Montomoli, C., Carosi, R., Massonne, H.-J., Langone, A., Visonà, D., 2015. Pressure–temperature–time–deformation path of kyanite-bearing migmatitic paragneiss in the Kali Gandaki valley (Central Nepal): investigation of late Eocene-early Oligocene melting processes. Lithos 231, 103–121.

Iaccarino, S., Montomoli, C., Carosi, R., Massonne, H.-J., Visonà, D., 2017. Geology and tectono-metamorphic evolution of the Himalayan metamorphic core: insights from the Mugu Karnali transect, Western Nepal (Central Himalaya). Journal of Metamorphic Geology 35, 301–325.

Iacopini, D., Carosi, R., Montomoli, C., Passchier, C.W., 2008. Strain analysis and vorticity of flow in the Northern Sardinian Variscan Belt: recognition of a partitioned oblique deformation event. Tectonophysics 446, 77–96.

Leake, B.E., Woolley, A.R., Arps, C.E.S., Birch, W.D., Gilbert, M.C., Grice, J.D., Hawthorne, F.C., Kato, A., Kisch, H.J., Krivivichev, V.G., Linthout, K., Laird, J., Mandarino, J.A., Maresch, W.V., Nickel, E.H., Rock, N.M.S., Schumacher, J.C., Smith, D.C., Stephenson, N.C.N., Ungaretti, L., Whittaker, E., Youzhi, G., 1997. Nomenclature of amphiboles: report of the subcommittee on amphiboles of the International Mineralogical Association, commission on new minerals and mineral names. European Journal of Mineralogy 9, 623–651.

Li, X.-H., Faure, M., Lin, W., 2014a. From crustal anatexis to mantle melting in the Variscan orogen of Corsica (France): SIMS U–Pb zircon age constraints. Tectonophysics 634, 19–30.

Li, Z., Yang, X., Li, Y., Santosh, M., Chen, H., Xiao, W., 2014b. Late Paleozoic tectono–metamorphic evolution of the Altai segment of the Central Asian Orogenic Belt: constraints from metamorphic P–T pseudosection and zircon U–Pb dating of ultra-high-temperature granulite. Lithos 204, 83–96.

Li, B., Massonne, H.-J., Opitz, J., 2017. Clockwise and anticlockwise P-T paths of high-pressure rocks from the 'La Pioza' eclogite body of the Malpica-Tuy zone, NW Spain. Journal of Petrology 58, 1363–1392.

Liou, J.G., Zhang, R.Y., Ernst, W.G., Rumble Douglas, I.I.I., Maruyama, S., 1998. High-pressure minerals from deeply subducted metamorphic rocks. In: Hemley, R.J. (Ed.), Ultrahigh-Pressure Mineralogy. Reviews in mineralogy vol. 37, pp. 33–96.

Massonne, H.-J., 2012. Formation of amphibole and clinozoisite-epidote in eclogite owing to fluid infiltration during exhumation in a subduction channel. Journal of Petrology 53, 1969–1998.

Massonne, H.-J., 2016a. Tertiary high-pressure metamorphism recorded in andalusite-bearing micaschist, southern Pirin Mts, SW Bulgaria. European Journal of Mineralogy 28, 1187–1202.

Massonne, H.-J., 2016b. Hydration of the lithospheric mantle by the descending plate in a continent–continent collisional setting and its geodynamic consequences. Journal of Geodynamics 96, 50–61.

Massonne, H.-J., Cruciani, G., Franceschelli, M., 2013. Geothermobarometry on anatectic melts – a high-pressure Variscan migmatite from Northeast Sardinia. International Geology Review 55, 1490–1505.

Massonne, H.-J., Cruciani, G., Franceschelli, M., Musumeci, G., 2018. Anticlockwise pressure–temperature paths record Variscan upper-plate exhumation: example from micaschists of the Porto Vecchio region. Corsica. Journal of Metamorphic Geology 36, 55–77.

Montomoli, C., 2003. Zone di taglio fragili-duttili nel basamento varisico metamorfico di basso grado della Nurra meridionale (Sardegna nordoccidentale). Atti della Società Toscana di Scienze Naturali, Memorie, serie A 108. pp. 23–29.

Newton, R.C., Charlu, T.V., Kleppa, O.J., 1981. Thermochemistry of the high structural state plagioclases. Geochimica et Cosmochimica Acta 44, 933–941.

Oggiano, G., Di Pisa, A., 1992. Geologia della Catena Ercinica in Sardegna La Zona Assiale. Struttura della Catena ercinica in Sardegna guida all'escursione. Gruppo informale di geologia strutturale, pp. 147–177 (Siena).

Pitra, P., Guiraud, M., 1996. Probable anticlockwise P-T evolution in extending crust: Hlinsko region, Bohemian Massif. Journal of Metamorphic Geology 14, 49–60.

Powell, R., Holland, T., 1999. Relating formulations of the thermodynamics of mineral solid solutions: activity modeling of pyroxenes, amphiboles, and micas. American Mineralogist 84, 1–14.

Ricci, C.A., Carosi, R., Di Vincenzo, G., Franceschelli, M., Palmeri, R., 2004. Unravelling the tectono-metamorphic evolution of medium-pressure rocks from collision to exhumation of the Variscan basement of NE Sardinia: a review. Special issue 2: a showcase of the Italian research in metamorphic petrology. Periodico di Mineralogia 73, 73–83.

Rossi, P., Oggiano, G., Cocherie, A., 2009. A restored section of the "southern Variscan realm" across the Corsica-Sardinia microcontinent. Comptes Rendus Geoscience 341, 224–238.

Tomkins, H.S., Powell, R., Ellis, D.J., 2007. The pressure dependence of the zirconium-in rutile thermometer. Journal of Metamorphic Geology 25, 703–713.

Vignaroli, G., Rossetti, F., Boubaouene, M., Massonne, H.-J., Theye, T., Faccenna, C., Funiciello, R., 2005. A counter-clockwise P-T path for the Voltri Massif eclogites (Ligurian Alps, Italy). Journal of Metamorphic Geology 23, 533–555.

von Raumer, J.F., Finger, F., Vesel, P., Stampfli, G.M., 2014. Durbachites-Vaugnerites – a geodynamic marker in the central European Variscan orogen. Terra Nova 26, 85–95.

Waizenhöfer, F., Massonne, H.-J., 2017. Monazite in a Variscan mylonitic paragneiss from the Münchberg Metamorphic complex (NE Bavaria) records Cadomian protolith ages. Journal of Metamorphic Geology 35, 453–469.

Watson, E.B., Wark, D.A., Thomas, J.B., 2006. Crystallization thermometers for zircon and rutile. Contributions to Mineralogy and Petrology 151, 413–433.

Xiang, H., Zhang, L., Zhong, Z.Q., Santosh, M., Zhou, H.W., Zhang, H.F., Zheng, J.P., Zheng, S., 2012. Ultrahigh-temperature metamorphism and anticlockwise P–T–t path of Paleozoic granulites from north Qinling–Tongbai orogen, Central China. Gondwana Research 21, 559–576.

Zack, T., Moraes, R., Kronz, A., 2004. Temperature dependence of Zr in rutile: empirical calibration of a rutile thermometer. Contributions to Mineralogy and Petrology 148, 471–488.

Please cite this article as: M. Scodina, G. Cruciani, M. Franceschelli, et al., Anticlockwise P-T evolution of amphibolites from NE Sardinia, Italy: Geodynamic implications for the..., Lithos, https://doi.org/10.1016/j.lithos.2018.12.003